RevMexAA (Serie de Conferencias), **15**, 237–242 (2003)

X-RAY OBSERVATIONS OF SUPERNOVA REMNANTS

J. Ballet

DSM/DAPNIA/SAp, CEA Saclay, France

RESUMEN

Los dos grandes observatorios de rayos-X en órbita proporcionan por primera vez espectros resueltos espacialmente de remanentes de supernova jóvenes a muy alta resolución espacial (*Chandra*) y muy alta sensibilidad (*XMM-Newton*). Los dos temas que han sacado más provecho de estos avances son: (1) Ahora tenemos mapas de la emisión de líneas de varios objetos, que muestran variaciones fuertes a escalas grandes y pequeñas. Esto refleja la distribución de los elementos y como fueron eyectados al instante de la explosión. (2) El gas ambiental chocado es ahora distinguido del gas eyectado, que es mucho más luminoso. Esto permite buscar las huellas específicas de la aceleración de rayos cósmicos en la onda de choque.

ABSTRACT

The two big X-ray observatories in orbit provide for the first time spatially resolved spectra of young supernova remnants, at very high spatial resolution (*Chandra*) and very high sensitivity (*XMM-Newton*). Two topics have benefitted most from these advances: (1) We now have maps of the line emission in several objects, showing strong variations at small and large scales. This reflects the distribution of the elements and how they were ejected at the time of the explosion. (2) The shocked ambient gas is now resolved from the much brighter ejecta. This allows us to look for specific signatures of cosmic-ray acceleration at the blast wave.

Key Words: **ACCELERATION OF PARTICLES — SUPERNOVA REMNANTS — X-RAYS: ISM**

1. INTRODUCTION

Supernova remnants (hereafter SNRs) are major actors in the interstellar ecosystem. They inject mechanical energy, heavy elements, and cosmic rays. Because the shock velocities range from hundreds to thousands of $\mathrm{km\,s^{-1}}$, the gas is heated to million-degree temperatures and shines preferentially in X-rays. X-ray observations are the best way to study the bulk of the thermal gas.

The *Chandra* (NASA) and *XMM-Newton* (ESA) satellites, both launched in 1999, are providing new insight into SNRs. Before 1999, we had reasonably good X-ray maps of SNRs (with *ROSAT* HRI) and reasonably good spectra (with *ASCA* SIS). But *ROSAT* HRI had no spectral resolution, and *ASCA* SIS had only modest spatial resolution ($30''$), not enough to resolve the bright young SNRs (a few arcminutes across) in detail. The CCDs on *Chandra* ACIS and *XMM* EPIC both offer spectral resolution comparable to *ASCA* SIS ($\simeq 100$ eV at 1 keV). *Chandra* has splendid spatial resolution ($0\farcs5$) allowing the resolution of very small-scale structures (which exist in SNRs). *XMM-Newton* has spatial resolution comparable to *ROSAT* ($6''$), but a large effective area ($2000\,\mathrm{cm^2}$ at 1 keV) permitting the study of spatial variations of the spectrum.

This review may be viewed as a complement to Decourchelle (2003). I have selected two topics which benefitted a lot from the improved capabilities. The first one (§ 2) is the spatial distribution of the elements freshly synthesized. The second one (§ 3) is the quest for how cosmic rays are accelerated at the blast wave.

2. HEAVY ELEMENTS IN YOUNG SNRS

In young supernova remnants, the main physical process is the interaction of high velocity material (ejecta) with the ambient medium (circumstellar or interstellar medium), giving rise to two shocks compressing and heating the matter. While the forward shock (or blast wave) propagates in the ambient medium, the reverse shock propagates back into the ejecta. These two adjacent shocked media, which constitute powerful X-ray emittors, are separated by a contact discontinuity and have different composition, density and temperature. As the ejecta are denser than the ambient medium and enriched in heavy elements, they dominate the X-ray emission with typical temperatures around 1 keV.

2.1. *Cas A and Core-Collapse Supernovae*

Cas A is the bright remnant from the explosion of a massive star, probably a Wolf-Rayet (Fesen, Becker, & Goodrich 1988), which has presumably been observed by Flamsteed in 1680. It is about $5'$

(or 5 pc) across. The *Chandra* image (Gotthelf et al. 2001) shows a wealth of substructure down to very small scales. The ejecta are very clumpy.

The color image of Cas A in three energy bands obtained with *Chandra* (Hughes et al. 2000) illustrates the range of spectral variations observed in the small-size knots, which originate from different nucleosynthesis burning zones. A twenty times deeper observation (Hwang, Holt, & Petre 2000) has allowed the distribution of the elements (Si, S, Ar, Ca, and Fe) to be mapped, and has confirmed that the iron-emitting ejecta is exterior to the silicon-emitting ejecta in the southeast region, but not elsewhere, implying a local inversion of the silicon-rich and innermost iron-rich ejecta layer. Maps of the abundances (Ne, Mg, Si, S, Ar, Ca, Fe, and Ni), derived from a detailed spectral modeling of the *XMM-Newton* data, confirm this result (Willingale et al. 2002). The observed abundances' behavior is qualitatively consistent with the expectation from current models of explosive nucleosynthesis.

The dynamics of the X-ray plasma has also been derived from Doppler velocity mapping of Cas A (Hwang et al. 2001; Willingale et al. 2002). The ejecta are globally distributed like a doughnut. That density enhancement possibly traces the equatorial plane of the progenitor. This was first seen with the *Einstein* FPCS (Markert et al. 1983), confirmed by the *ASCA* SIS (Holt et al. 1994) at low spatial resolution, and can now be analyzed in detail.

Another example of such a clumpy, O-rich remnant, is G292.0+1.8 (Park et al. 2002). It is 7′ across and somewhat older (> 1000 years), and contains a pulsar wind nebula. Differences between the elements (particularly Ne and Si) are also seen. A distinct difference with Cas A is that the image of G292.0+1.8 is crossed by a bright ridge of emission which has nothing to do with the ejecta structure (it has weak abundances), but is probably due to an equatorial belt in the progenitor's wind.

The ultimate fate of such SNRs could be something like Vela (5° across). In Vela, it was shown by *ROSAT* (Aschenbach, Egger, & Trumper 1995) that clumps have overtaken the blast wave and are now creating independent bowshocks in the ambient medium. A recent observation of one clump with *Chandra* (Miyata et al. 2001) has shown that it has decidedly non-Solar abundances (Si rich, O poor).

2.2. *Remnants of Thermonuclear Explosions*

The remnant of Tycho (SN 1572), which is considered as the prototype for Type Ia supernova remnants, has been observed with *XMM-Newton* (Decourchelle et al. 2001). With an angular diameter of about 8′, Tycho is well suited for mapping the distribution of heavy elements in the ejecta of a Type Ia supernova. There is a strong asymmetry in the line emission with the northwestern side being the brightest and the southeastern side the faintest. Conversely, the continuum emission is rather homogeneous, more extended than the line emission and is mostly attributed to the shocked ambient medium.

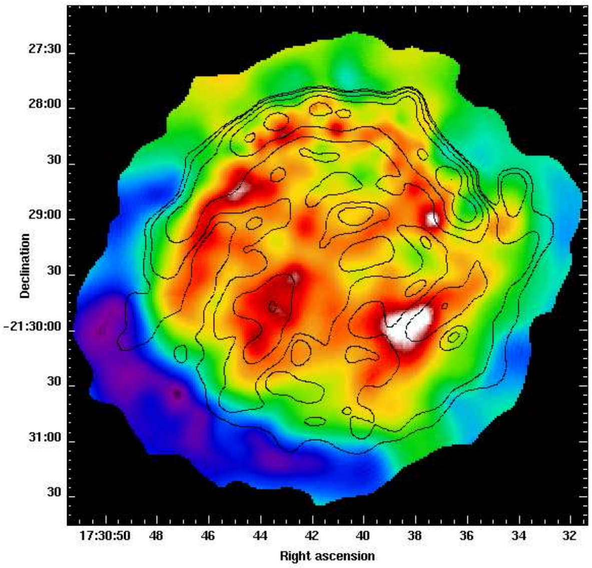

Fig. 1. Map of the equivalent width of the Fe K line in Kepler's SNR (Cassam-Chenaï et al. 2003) obtained with *XMM-Newton*. The line and continuum maps were adaptively smoothed before division to a signal to noise of 11. The color coding runs linearly from 0 (not significant, outside the remnant) to 7.7 keV. The contours trace the brightness in the Fe K line. The area of low equivalent width to the south east is mostly ambient medium. The rest is dominated by the ejecta. There is no obvious correlation between brightness and equivalent width, contrary to what is seen in Cas A and Tycho.

The regular spherical emission of the continuum indicates that the medium surrounding the Tycho supernova remnant is fairly homogeneous, which is in agreement with the results from a search for H I clouds in the vicinity of the remnant (Reynoso et al. 1999). As a result, the asymmetry observed solely in the lines is attributable to the ejecta, and not to the structure of the medium surrounding the remnant. The difference in the emission between the northeastern and southwestern regions is related either to different temperatures and/or to a different composition of the ejecta. This result challenges the supernova Ia explosion models, as they are not expected to produce such asymmetry.

The comparison between the spatial distribution of Si K and Fe L lines shows a similar global morphology between them, except in the southeastern knots where spatial variations of the relative abundance of silicon and iron are observed (Vancura, Gorenstein, & Hughes 1995) and now confirmed by a spectral analysis. In contrast to the globally spatially coincident emission of Si K and Fe L, the Fe K emission clearly peaks at a smaller radius (Hwang & Gotthelf 1997) and indicates a higher temperature toward the reverse shock. The higher temperature toward the interior is qualitatively consistent with the propagation of the reverse shock in the central plateau of the ejecta. An exponential initial density profile, prefered for Type Ia, gives a temperature profile flatter than the temperature gradient required to fit the X-ray spectrum of Tycho, unless circumstellar material is present.

The remnant of Kepler (SN 1604), twice as far away, is at first sight very similar to that of Tycho. It has also been observed with *XMM-Newton*. But in Kepler the continuum map shows the same asymmetry as the line maps. Figure 1 shows the map of the equivalent width in the Fe K line. Except the south-east region (where the iron abundance is clearly lower than elsewhere), the rest of the map is rather flat and, in particular, no correlation is seen with the flux. This points at an external origin for the asymmetry, for example a higher ambient density to the north and north-west, and is reminiscent of the bowshock model proposed on the basis of optical observations (Bandiera 1987).

3. COSMIC-RAY ACCELERATION IN SNRS

Supernova remnants are considered as the site of acceleration of Galactic cosmic rays up to energies of 10^{15} eV. Particles gain energy (first-order Fermi acceleration) by diffusing back and forth across the shock on the inhomogeneities of the magnetic field (Drury 1983). The observation of synchrotron radio emission indicates that electrons are being accelerated at least up to energies of about 10^9 eV in supernova remnant shells.

3.1. *Dynamic Effects*

If a significant fraction of the supernova energy goes into accelerating particles, this results in a modification of the shock structure, which impacts the overall hydrodynamics and thermal emission of the remnant (Decourchelle, Ellison, & Ballet 2000).

For the first time, the emission from the forward shock has been resolved (Gaetz et al. 2000) and the X-ray spectrum of the post-shock region has been measured (Hughes, Rakowski, & Decourchelle 2000) using the *Chandra* observation of the remnant of 1E 0102.2−7219 in the Small Magellanic Cloud. As the distance to this remnant is well known, the determination of the post-shock electron temperature and proper motion of 1E 0102.2−7219 can be used to constrain the efficiency of the acceleration at this shock. Indeed, for efficient acceleration the shock jump conditions are modified (Drury 1983). For a given shock velocity, the compression ratio is increased while the post-shock temperature is decreased compared to the test-particle case (for which there is no feedback of the accelerated particles).

The derived expansion rate implies a blast-wave velocity of $\simeq 6000\,\mathrm{km\,s^{-1}}$ at the distance of the Small Magellanic Cloud. Depending on the degree of collisionless electron heating, the post-shock electron temperature is expected to be in the range 2.5 to 45 keV. The *Chandra* spectrum reveals an electron temperature in the range 0.4 to 1 keV, which is much lower than the expected temperature. This can only be understood if a significant fraction of the energy went into accelerating cosmic rays. Efficient acceleration alone could account for the measured low value of the electron post-shock temperature without invoking non-equipartition between the electron and ion temperatures.

3.2. *The Outer Rim*

Thanks to its very high spatial resolution, *Chandra* has the ability to resolve the outer blast wave in SNRs. Both in Cas A (Gotthelf et al. 2001) and in Tycho (Hwang et al. 2002), a very sharp peak in the continuum emission was noticed exactly at the blast wave. This is illustrated in Figures 2 and 3. The outer rim is only 3 to 4″ broad in both remnants, which amounts to only 2% of the radius. The spectrum does not allow us to deduce the origin of that peak. It is mostly featureless but this could be due to a very strong ionization lag.

However, it is very hard to imagine how thermal gas could behave in that way. There is no evidence (optical or UV) for a radiative shock, and no dynamic model of an adiabatic SNR predicts such a sharp density drop behind the shock, particularly in projection. The Sedov model has a strong density peak at the shock, but this still results in a rather broad peak (10% of the radius, before projection). Reverse-shock models tend to be even less contrasted.

On the other hand, such a peak may be interpreted more naturally in the framework of a non-

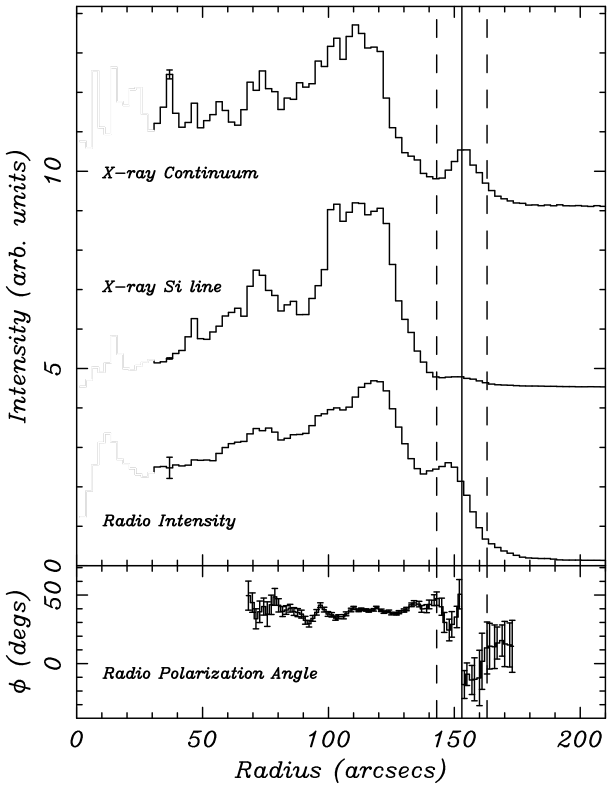

Fig. 2. Radial profiles at the external rim in Cas A (Gotthelf et al. 2001) obtained with *Chandra*. The blast wave is marked by the onset of radio polarization and a sharp ridge in the X-ray continuum. No such ridge is present in the line emission nor in the radio brightness. The radio brightness in particular rises steeply but does not decrease behind the blast wave as the X-ray continuum does.

thermal (synchrotron) model (Reynolds 1998) if radiative losses are such that the electrons are energetic enough to radiate in X-rays only at the shock front. Indeed, radio maps do not seem to exhibit such sharp peaks. Quantitatively, the synchrotron cooling time is

$$t_{\rm cool} = 6.37 \times 10^2\, B^{-2} E^{-1}\,{\rm s}, \tag{1}$$

where B is the magnetic field strength (Gauss) and E is the electron energy (erg). The frequency at which an electron radiates preferentially is

$$\nu_{\rm sync} = 1.82 \times 10^{18} B E^2\,{\rm Hz}. \tag{2}$$

Imposing $\nu_{\rm sync} = 2.42 \times 10^{17}$ Hz (1 keV, to be in the X-ray regime), and eliminating E from equations (1,2), one gets the synchrotron cooling time for X-ray emitting electrons $t_{\rm cool} = 1.75 \times 10^3 B^{-3/2}$ s.

At 3.4 kpc (Cas A), $3''$ correspond to $\Delta r = 1.53 \times 10^{17}$ cm. The time it takes for the gas to move away from the shock over that distance is

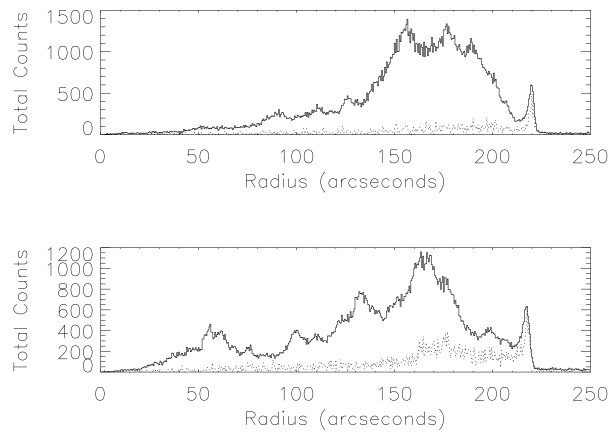

Fig. 3. Radial profiles of the X-ray brightness in Tycho (Hwang et al. 2002) obtained with *Chandra*. In both plots, the solid line shows the broad-band emission, the dotted line shows the continuum emission (4 to 6 keV) alone. The two figures correspond to two azimuths (top: toward the north-west; bottom: toward the south-west). The sharp ridge following the blast wave is even more striking than in Cas A.

$$\Delta t = \frac{R\,\Delta r}{v_{\rm sh}} \simeq 1.76 \times 10^9\,{\rm s}, \tag{3}$$

where R is the compression ratio at the shock (assumed to be 4) and $v_{\rm sh}$ is the shock speed, estimated from the maximum measured velocity $v_{\rm max} = 2600\,{\rm km\,s^{-1}}$ (Willingale et al. 2002) via $v_{\rm max} = (1 - 1/R)\, v_{\rm sh}$. Equating Δt to $t_{\rm cool}$, one gets $B \simeq 100\,\mu$G behind the shock. This is reasonable but much larger than interstellar values, giving observational weight to the idea that the magnetic field may be amplified in the particle acceleration process (Lucek & Bell 2000).

3.3. *Synchrotron-Dominated X-Ray Emission*

The discovery of synchrotron X-ray emission with *ASCA* in the shell-like remnant of SN 1006 (Koyama et al. 1995), has shown the existence of electrons with energies of $\simeq 10^{14}$ eV, confirmed by the detection of TeV γ-ray emission (Tanimori et al. 1998). X-ray observations of SN 1006 with *XMM-Newton* and *Chandra* give unique information on the variation and characteristics of the synchrotron emission. This information is crucial for constraining the models of particle acceleration, in particular to investigate the dependence of the acceleration efficiency on the magnetic field orientation. Images are presented in Decourchelle (2003).

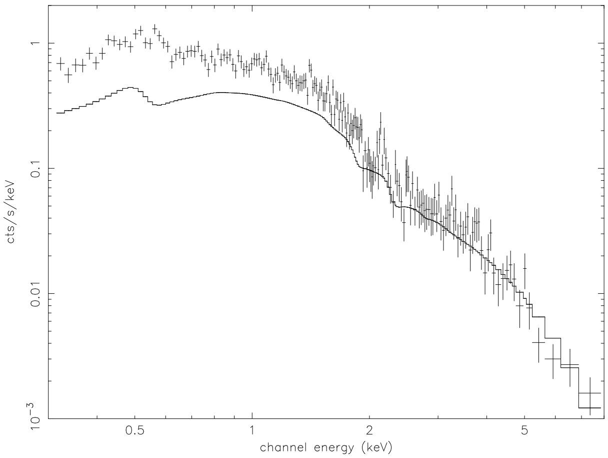

Fig. 4. *XMM-Newton* EPIC MOS spectrum of the north-east bright limb of SN 1006 (Rothenflug et al. 2003). The synchrotron component (solid line) dominates but thermal emission (in particular the O Heα line at 570 eV) can still be seen.

To characterize the broad-band synchrotron emission, the X-ray data need to be fitted together with the radio data, which give both the normalization and spectral index of the synchrotron emission (Figure 4). This is required to determine the break frequency at higher energy of the synchrotron spectrum and its spatial variations. The combined Molonglo and single dish Parkes radio data (Roger et al. 1988) ensures that no flux is lost at low spatial frequencies. The azimuthal variations of the break frequency are then measured for the first time in a supernova remnant and are shown in Figure 5.

Previously, the spectrum of only the global north-east bright limb was accessible with *ASCA* data (Dyer et al. 2001). The *XMM-Newton* azimuthal profile is compared with the escape model (Reynolds 1998) used in that work, which is justified because of the low value of the magnetic field ($\simeq 10\,\mu$G) inferred from the TeV observations (Tanimori et al. 1998). This model assumes that the cosmic-ray acceleration is independent of the magnetic field orientation, so that the cut-off electron energy is identical all along the shock. The variations in flux and break frequency are then attributed to the variations of the magnetic compression at the shock and behind, as a function of the angle between the magnetic field and the shock normal (assuming Sedov dynamics).

As is shown in Fig. 5, the projected model is too flat to account for the observed azimuthal variations, even for a magnetic field in the plane of the sky which maximizes the break frequency variations with azimuth. If the magnetic field is inclined with respect to the line of sight by 60 degrees (Reynolds 1996), the azimuthal variations of the break frequency become even harder to reproduce. Variations of the magnetic compression alone are unable to explain the observed azimuthal variations. This implies that the maximum energy reached by accelerated particles is higher at the bright limbs than elsewhere, reaching at least a value of 70 TeV (assuming a magnetic field of $10\,\mu$G).

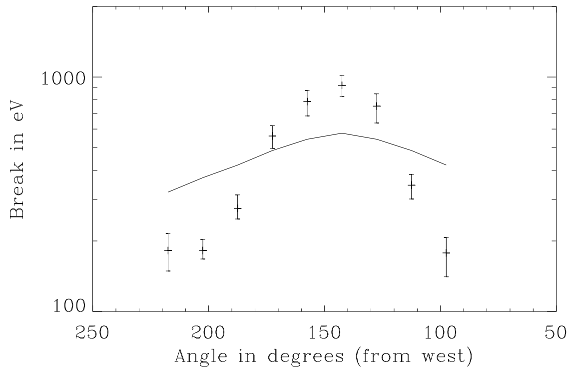

Fig. 5. Observed variations of the cut-off frequency of the synchrotron component as a function of azimuth in SN 1006. The solid line shows the profile expected from the escape model of Reynolds (1998), which assumes that the variations of the cut-off frequency depend only on the compression of the magnetic field as a function of the angle with the shock normal.

Another shell-type supernova remnant is, as in SN 1006, dominated by nonthermal processes: G347.3−0.5 (Slane et al. 1999). This one has a much more complex environment than SN 1006 (it is close to the Galactic plane). Its radio emission is weak and confused. Its γ-ray emission was recently the subject of vigorous debate (Enomoto et al. 2002; Reimer & Pohl 2002; Butt et al. 2002). Figure 6 shows the mosaic of a recent set of *XMM-Newton* observations. A quiet (no pulsar wind nebula) neutron star is seen. The diffuse X-ray emission is entirely non-thermal (Figure 7), with no trace of any thermal emission anywhere. This probably means that the ambient density is even lower than around SN 1006 (the X-ray emission per unit volume is proportional to n_e^2 and decreases very fast with density).

4. CONCLUSIONS

The data collected on supernova remnants with *XMM-Newton* and *Chandra* satellites are providing a wealth of new results, giving a new insight into the physics of the supernova remnants. In particular, the ability of CCDs to provide spatially resolved spectroscopy, even at a limited spectral resolution, is essential to investigate the complex emission and morphology of these objects.

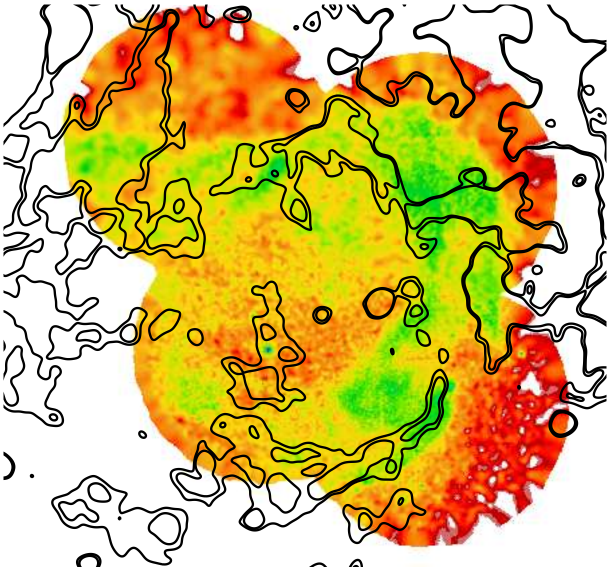

Fig. 6. Brightness map of the X-ray emission (2 to 4.5 keV) in the SNR G347.3−0.5 (Cassam-Chenaï et al. 2003), obtained with *XMM-Newton*. The contours trace the radio continuum emission (MOST, 843 MHz). The morphology is very complex due to the structure of the ambient medium (several molecular clouds abutt the SNR).

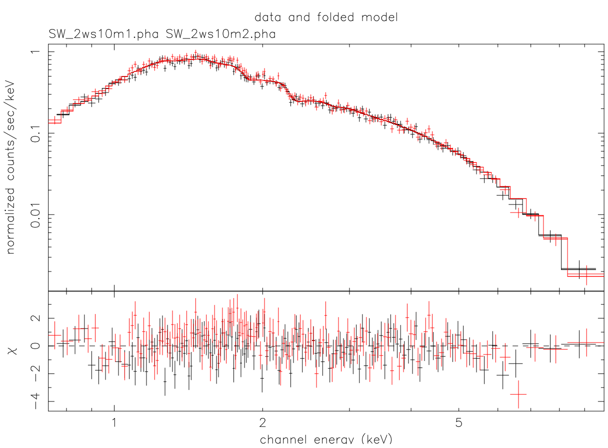

Fig. 7. *XMM-Newton* EPIC MOS spectrum of a region in the south-west of G347.3−0.5. The spectrum is entirely non-thermal. The solid line shows an absorbed power-law fit ($N_{\rm H} = 8 \times 10^{21}\,{\rm cm}^{-2}$, $\Gamma = 2.4$).

REFERENCES

Aschenbach, B., Egger, R., & Trumper, J. 1995, Nature, 373, 587
Bandiera, R. 1987, ApJ, 319, 885
Butt, Y. M., Torres, D. F., Romero, G. E., Dame, T. M., & Combi, J. A. 2002, Nature, 418, 499
Cassam-Chenaï, G., et al. 2003, in preparation
Decourchelle, A. 2003, in ESA SP-488, New Visions of the X-ray Universe in the *XMM-Newton* and *Chandra* Era, ed. F. Jansen (Noordwijk: ESTEC-ESA), in press
Decourchelle, A., Ellison, D. C., & Ballet, J. 2000, ApJ, 543, L57
Decourchelle, A., et al. 2001, A&A, 365, L218
Drury, L. O'C. 1983, Rep. Prog. Phys., 46, 973
Dyer, K. K, Reynolds, S. P., Borkowski, K. J., Allen, G. E., & Petre, R. 2001, ApJ, 551, 439
Enomoto, R., et al. 2002, Nature, 416, 823
Fesen, R. A., Becker, R. H., & Goodrich, R. W. 1988, ApJ, 329, L89
Gaetz, T. J., et al. 2000, ApJ, 534, L47
Gotthelf, E. V., Koralesky, B., Rudnick, L., Jones, T. W., Hwang, U., & Petre, R. 2001, ApJ, 552, L39
Holt, S. S., Gotthelf, E. V., Tsunemi, H., & Negoro, H. 1994, PASJ, 46, L151
Hughes, J. P., Rakowski, C. E., Burrows, D. N., & Slane, P. O. 2000, ApJ, 528, L109
Hughes, J. P., Rakowski, C. E., & Decourchelle, A. 2000, ApJ, 543, L61
Hwang, U., Decourchelle, A., Holt, S. S., & Petre, R. 2002, ApJ, 581, 1101
Hwang, U., & Gotthelf, E. V. 1997, ApJ, 475, 665
Hwang, U., Holt, S. S., & Petre, R. 2000, ApJ, 537, L119
Hwang, U., Szymkowiak, A. E., Petre, R., & Holt, S. S. 2001, ApJ, 560, L175
Koyama, K., et al. 1995, Nature, 378, 255
Lucek, S. G., & Bell, A. R. 2000, MNRAS, 314, 65
Markert, T. H., Clark, G. W., Winkler, P. F., & Canizares, C. R. 1983, ApJ, 268, 134
Miyata, E., Tsunemi, H., Aschenbach, B., & Mori, K. 2001, ApJ, 559, L45
Park, S., et al. 2002, ApJ, 564, L39
Reimer, O., & Pohl, M. 2002, A&A, 390, L43
Reynolds, S. P. 1996, ApJ, 459, L13
———. 1998, ApJ, 493, 375
Reynoso, E. M., Velázquez, P. F., Dubner, G. M., & Goss, W. M. 1999, AJ, 117, 1827
Roger, R. S., Milne, D. K., Kesteven, M. J., Wellington, K. J., & Haynes, R. F. 1988, ApJ, 332, 940
Rothenflug, R., et al. 2003, in preparation
Slane, P., et al. 1999, ApJ, 525, 357
Tanimori, T., et al. 1998, ApJ, 497, L33
Vancura, O., Gorenstein, P., & Hughes, J. P. 1995, ApJ, 441, 680
Willingale, R., Bleeker, J. A. M., van der Heyden, K. J., Kaastra, J. S., & Vink, J. 2002, A&A, 381, 1039

Jean Ballet: Service d'Astrophysique, Bt 709, CEA Saclay, 91191 Gif sur Yvette Cedex, France (jballet@cea.fr).